13. Mazets, E. P., *et al.*, *Astrophys. Space Sci*, 1982, **82**, 261–282
14. Murakami, T., *Nature*, 1988, **335**, 234–235.
15. Liang, E. P., *Astrophys. J.*, 1986, **304**, 682–687
16. Helfand, D. J. and Long, K. S, *Nature*, 1979, **282**, 589–591.
17. Pizzhichini, G., *et al.*, *Astrophys. J*, 1986, **301**, 641–649.
18. Pederson, H., *et al.*, *Astrophys J. Lett.*, 1983, **270**, L43–47.
19. Barat, C., *et al.*, *Astrophys. J.*, 1984, **280**, 150–153.
20. Laros, J. G., *et al.*, *Astrophys. J.*, 1985, **290**, 728–734
21. Motch, C. *et al.*, *Astron. Astrophys.*, 1985, **145**, 201–205.
22. Hartmann, D. H. and Pogge, R. W, *Astrophys. J*, 1987, **318**, 363–369.
23. Atteia, J. L., *et al.*, *Astrophys. J. Suppl*, 1987, **64**, 305–382.
24. Mazets, E. P., *et al.*, *Astrophys. Space Sci.*, 1981, **80**, 3–143
25. Beurle, K., *et al.*, *Astrophys. Space Sci.*, 1981, **77**, 201–214
26. Meegan, C. A., *et al*, *Astrophys. J*, 1985, **291**, 479–485.
27. Proceedings of the GRO Science Workshop, NASA (ed Johnson, W. N.), 1989.
28. Fishman, G. J, *et al.*, in AIP Conference Proceedings (eds Paciesas, W. S. and Fishman, G. J), 1992, p. 13.
29. Hurley, K., *et al.*, *Nature*, 1994, **372**, 652.
30. Koveliotou, C., IAU Circ. 5567 & 5592, 1992.
31. Teegarden, B J., *et al*, *BAAS*, 1991, **23**, 1470.
32. Palmer, D. M., *et al*, *BAAS*, 1992, **24**, 1259
33. Schaefer, B. E, *et al*, in AIP Conference Proceedings (eds Paciesas, W. S. and Fishman, G J), 1992, p. 180.
34. Band, D., *et al.*, *BAAS*, 1992, **24**, 1258
35. Meegan, C. A., *et al.*, *Nature*, 1992, **355**, 143.
36. Meegan, C. A, *et al.*, in AIP Conference Proceedings No 307 (eds Fishman G. J. *et al*), 1994, p. 3.
37. Harwit, M. and Salpeter, E, *Astrophys J. Lett*, 1973, **186**, 37.
38 Schklovskii, I., *Soviet Astronomy*, 1974, **51**, 665.
39. Woosley, S. and Taam, R, *Nature*, 1976, **263**, 101.
40. Li, H. and Dermer, C. D, *Nature*, 1992, **359**, 514.
41. Pacini, F. and Ruderman, M, *Nature*, 1974, **251**, 399.
42. Paczynski, B., *Astrophys. J Lett.*, 1986, **308**, L43
43. Narayan, R., Paczynski, B. and Piran, T., *Astrophys. J. Lett*, 1992, **395**, L83.
44. Norris, J. P., *et al*, *Astrophys. J.*, 1994, **424**, 540–545.
45. Cline, T. L., *et al*, *Astrophys. J. Lett.*, 1984, **286**, L15–18.
46. Rothschild, R E., *et al.*, *Nature*, 1994, **368**, 432.
47. Koveliotou, C, *et al.*, *Nature*, 1994, **368**, 125.
48. Kulkarni, S. R., *Nature*, 1993, **365**, 33.
49. Cooke, B. A, *Nature*, 1993, **366**, 413.
50. Murakami, T., *et al.*, *Nature*, 1994, **368**, 127
51. Hurley, K. *et al.*, *Astrophys. J*, 1994, **431**, L31.
52. Shaefer, B. E., in AIP Conference Proceedings No. 307 (eds Fishman, G. J, *et al.*), 1994, p. 382.
53. Hudec, R., *Astron. Lett. Comm.*, 1993, **28**, 359.
54. Kippen, R. M., *et al.*, in AIP Conference Proceedings No. 307 (eds Fishman, G. J. *et al.*), 1994, p. 418.
55 Hurley, K., in AIP Conference Proceedings No. 280 (eds Friedlander, M., Gehrels, N. and Macomb, D. J), 1993, p 769.
56 Barat C., *A&A Suppl.*, 1993, **97**, 43–48.
57. Hurley, K, *A&A Suppl.*, 1992, **92**, 401–410.
58 Owens, A., *et al.*, *IEEE-NS*, 1991, **38**, 559–567.
59. Marar, T. M. K, *et al*, *A&A*, 1994, **283**, 698.
60. Ramakrishna Sharma, M R., *et al.*, *IEEE NS*, 1993, **40**, 1989–1997.
61. Marar, T. M. K, *et al.*, *J. Spacecraft Technol.*, 1995, **5**, 75.
62. Kasturirangan, K, *et al.*, *A&A*, 1994, **283**, 435.
63 Hurley, K., in AIP Conference Proceedings No. 307 (eds Fishman G J. *et al*), 1994, p. 359.
64. Ricker, G., *et al.*, in *Gamma Ray Bursts*, Cambridge University Press, 1992, p. 288.

ACKNOWLEDGEMENTS. We thank the staff of the Technical Physics Division for their unstinted efforts during the payload development. Thanks are also due to the SROSS project team and the staff of the satellite tracking centre (ISTRAC) for their continuing support in the payload operations.

Received 12 August 1995, accepted 27 September 1995

Quantum Monte Carlo techniques: Chemical applications

Charusita Chakravarty

Department of Chemistry, Indian Institute of Technology, New Delhi 110 016, India

Quantum Monte Carlo (QMC) methods are stochastic simulation methods for quantum many-body systems. Here we provide an overview of QMC methods designed for simulation of atomic and molecular systems, and discuss main ideas behind the variational, diffusion and path integral QMC methods. We also review application of these techniques to some problems of interest in chemistry.

> The underlying physical laws necessary for the mathematical theory of a large part of physics and the whole of chemistry are (thus) completely known, and the difficulty is only that the exact application of these laws leads to equations much too complicated to be solvable. It therefore becomes desirable that approximate practical methods of applying quantum mechanics should be developed, which can lead to an explanation of the main features of complex atomic systems without too much computation.

SINCE P. A. M. Dirac wrote the above lines in 1929 (ref. 1), both the range of approximate quantum mechanical methods, and the notion of what constitutes 'too much computation' have undergone dramatic changes.

Over the past few decades, chemists have come to understand the interactions and dynamics of small molecules and clusters very well. Both theory and experiment can, for instance, provide a very accurate

understanding of the H_2O molecule and a reasonable one of the dimeric and trimeric aggregates $(H_2O)_2$ and $(H_2O)_3$ (refs 2,3). The macroscopic end of the scale, such as the thermodynamics and spectroscopy of bulk liquids and solids is again well understood from a phenomenological point of view; for example, bulk water is known to be a complex fluid with an elaborate phase diagram[4]. The conceptual connection between microscopic and macroscopic behaviour is made by statistical mechanics. Computer simulation methods complement the elegant but simplified statistical mechanical models by providing a much clearer connection between experimental and calculated quantities, the ability to make quantitative or semiquantitative predictions and the opportunity for performing numerical or computer experiments for systems or conditions which may not be easily realizable in a laboratory.

Currently, most simulations are performed using either classical Monte Carlo methods or the molecular dynamics approach[5]. Applications of these methods range from geochemistry to protein structure[6,7]. Both techniques assume the Born–Oppenheimer separation of electronic and nuclear motion. The nuclei are assumed to be classical particles moving according to the Newtonian equations of motion on the electronic potential energy surface (PES). The PES itself is constructed as a sum of pair (or at most three- and four-body) interactions between atoms, i.e. the total interaction energy of a system is assumed to be the sum of the interaction energies between all unique pairs. These few-body potentials are derived from independent studies of small aggregates and provide the necessary simulation input about the details of the microscopic interaction[8]. Classical Monte Carlo techniques generate the equilibrium statistical mechanical properties of a system, usually within the canonical ensemble, such as the average potential energy, structural quantities such as the radial distribution function and phase transition behaviour. For an N-atom system, such Monte Carlo techniques construct a random walk through the $3N$-dimensional configuration space with a bias such that for sufficiently long walks, a set of configurations, $\mathbf{x}$, distributed according to the Boltzmann formula $e^{-\beta V(x)}$ is generated. If N is sufficiently large and suitable boundary conditions are applied, then equilibrium properties of the bulk system can be generated. MC integration is an inherently multidimensional approach with a statistical accuracy in the results that is proportional to $(n/\tau)^{1/2}$, where n is the number of MC configurations and τ is a measure of the degree of correlation between successive configurations. While τ does tend to increase with dimensionality of the system, this dependence is generally small. Consequently, MC methods scale relatively favourably with system size, in terms of computational cost.

Classical molecular dynamics, instead of using a random walk approach, involves numerical integration of the classical equations of motion to generate the trajectory of the N-particle system through phase space. Provided certain conditions are satisfied (ergodicity, sufficient length of trajectory and the like), the phase space points sampled during the course of an MD run provide information on both the equilibrium and dynamical statistical mechanical quantities. Thus, unlike MC, MD methods can provide time-correlation functions related to transport properties and spectroscopy. However, MD can prove inefficient relative to MC for systems with multiple time scales. For example, in binary solid solutions, the rates of diffusion of the two species are much slower than the high frequency lattice vibrations[9].

An important development in the past decade has been the formulation of *ab initio* MD methods, which attempt to overcome the problems of inadequate parametrization of the PES surface. Such problems are most acute in the case of semiconductor and metal systems; the delocalized nature of the valence electrons in such materials implies that the pair potential approximation is very poor. This is also true for chemical reactions where changes in electronic structure and nuclear configuration are very strongly correlated. Polarizability effects are also notoriously hard to incorporate within a pair potential approach. The *ab initio* MD methods attempt to solve this problem by solving the electronic structure problem simultaneously with the integration of the classical equations of motion and, in principle, require no input other than electronic and nuclear masses and electric charges.

The most successful *ab initio* MD approach to date is the Car–Parinello (CP) formulation. The CP technique uses the Born–Oppenheimer approach to separate motion of the ionic cores from that of the valence electrons. The motion of ionic cores is treated by using classical MD equations of motion. To obtain a suitable electronic PES, the ground state electronic energy for any given ionic configuration must be found. To do this both accurately and efficiently, three important simplifications are made: (i) Density functional theory (DFT) is used to model electron–electron interactions. DFT is a mean-field approach which introduces electron correlation effects in an approximate way. Results for a variety of ground state properties using DFT have been shown to be accurate to within a few per cent. (ii) Pseudopotential theory is used to model electron–ion interactions. Pseudopotentials smooth out the strongly varying regions of the potential for small ion–electron distances while retaining the salient characteristics of valence electron in a bulk medium. (iii) Dynamical minimization techniques are based on the insight that the variational solution to the density functional equations can be obtained by a constrained optimization scheme in which basis functions for the electronic structure problem are

treated as dynamical variables. The advantage of this approach is that the real-time dynamics of the ionic cores and the fictitious dynamics associated with the electronic variables can be coupled together in a very powerful computational scheme. The net result is that the classical motion of atoms on the ground state Born–Oppenheimer PES is obtained. The CP method has provided remarkable results for many problems of current interest in materials science[10]. The technique is at least an order of magnitude more expensive than classical MD.

Quantum Monte Carlo (QMC) methods, as the name suggests, are stochastic simulation methods for quantum many-body systems[11–16]. The term QMC covers a battery of techniques used in a variety of fields such as condensed matter physics, nuclear physics, statistical mechanics and chemistry. This review is intended to provide an overview of QMC methods designed for simulation of atomic and molecular systems of interest in chemistry.

One situation in which QMC methods become essential for chemical systems is when the atomic nuclei are sufficiently light or temperatures are sufficiently low that the approximation of treating nuclear motion classically becomes a poor one. For example, quantum effects are important in the water and ice because of hydrogen-bonding. Electron and proton transfer processes, vital to many biochemical processes, are intrinsically quantum mechanical. Many solids such as ammonium halides and solid H_2 show phase transitions, with large isotope effects indicative of strong quantum effects[4]. Even solid argon must be modelled with significant quantum corrections to thermodynamic properties[5].

Electronic structure problems are a second area of chemistry where QMC methods are applicable when accuracy requires improvements over density functional theory (the basis of Car–Parrinello) or when the Born–Oppenheimer approximation fails due to strong coupling between nuclear and electronic motion[13].

The review is organized as follows. Sections 1, 2 and 3 present the essential ideas behind the variational, diffusion and path integral Monte Carlo methods respectively. Section 4 briefly reviews the application of QMC methods to some problems of interest in traditional chemistry where the simulations provide interesting insights and connections between experimental data and simplified theoretical models.

1. Variational quantum Monte Carlo methods

The variational Monte Carlo (VMC) approach is based on the variation principle which states that for a given Hamiltonian $\hat{H}$, the energy E_t associated with a trial wavefunction ψ_t, defined as

$$E_t = \int \psi_t^* \hat{H} \psi_t \, d\tau / \int \psi_t^* \psi_t \, d\tau \qquad (1)$$

will always be greater than or equal to the exact ground state energy E_0 of the system[12]. Minimizing E_t with respect to the parameters of ψ_t provides the best approximation to the ground state wavefunction within the limitations of a given functional form. Conventional quantum chemical methods expand the trial wavefunction ψ_t as a linear combination of a suitable set of basis functions and then utilize the variation theorem to obtain the optimum set of linear combinations. While such methods can provide very accurate energies and wavefunctions, they scale very inefficiently with the system size or dimensionality. For example, configuration interaction methods scale as N^7, where N is the number of basis functions, implying that such studies are only feasible for small molecules.

VMC methods use the favourable scaling of Monte Carlo methods with system size by interpreting $\psi_t^* \psi_t$ as a probability distribution. Standard random walk methods can be used to create a set of configurations, $\mathbf{x}$, distributed according to $\psi_t^*(\mathbf{x}) \psi_t(\mathbf{x})$ and E_t can be defined as the average over this set of configurations of the local energy, $E_t = \hat{H} \psi_t(\mathbf{x})/\psi_t(\mathbf{x})$. The form of the trial wavefunction is usually derived from a knowledge of the basic physics of the problem and the parameters can then be optimized by minimizing E_t or, better still, the variance in E_t.

VMC methods are computationally relatively inexpensive and can provide considerable physical insight. The limitations of VMC methods are two-fold: (i) the accuracy of the calculation is limited by the choice of functional form of ψ_t; (ii) being essentially a ground state method, information on excited state energies and wavefunctions is difficult to obtain though not impossible. Despite these limitations, VMC calculations are capable of providing accurate results for a variety of systems. As an example of an application to solid state electronic structure calculation, the bulk cohesive energy of diamond and graphite was calculated to within 1% of the experimental value using VMC[17]. VMC simulations of helium have provided very accurate results, when compared with experiment, for properties of helium in the bulk, at surfaces and in droplets[18].

2. Diffusion Monte Carlo methods

Diffusion Monte Carlo (DMC), like VMC, is a zero-temperature approach that is geared towards finding the ground state wavefunction. Unlike VMC, which provides an upper bound to the ground state energy, DMC is, in principle, capable of generating the *exact* ground state energy and wavefunction[11–16].

The starting point of the DMC method is the time-dependent Schrödinger equation

$$i\hbar \frac{\partial \Psi}{\partial t} = \hat{H} \Psi , \qquad (2)$$

where t is the time coordinate. If t is treated as an imaginary quantity $t = -iu$ (where u is real), then the above equation can be rewritten as:

$$-\hbar \frac{\partial \Psi}{\partial u} = \hat{H}\Psi , \tag{3}$$

or

$$\Psi_{final} = e^{-u\hat{H}/\hbar} \Psi_{initial} . \tag{4}$$

By an analogy with the density operator, $e^{-\beta\hat{H}}$, used in statistical mechanics, imaginary time in the above equation can be interpreted as proportional to the inverse temperature, $\beta = 1/k_B T$ such that $u = \beta\hbar$, T is the absolute temperature and k_B is the Boltzmann constant. It can be shown that regardless of the choice of $\Psi_{initial}$, Ψ_{final} will converge exponentially to the ground state wavefunction Ψ_0 with energy E_0 in the limit $\beta \to \infty$, $T \to 0$. If it is assumed that the ground state wavefunction is nodeless, as is the case for bosons or distinguishable particles, then the above equation can be interpreted as the evolution of an initial, arbitrary probability distribution to the final stationary state distribution given by Ψ_0. To understand the basis of the computational scheme, consider the evolution of the distribution over a very small imaginary time interval, $\varepsilon = \beta/M$, from time u_i to u_{i+1}. Then it is possible to factorize $e^{-\beta\hat{H}/M}$ as $e^{-\beta\hat{K}/M}$ $e^{-\beta\hat{V}/M}$, where $\hat{K}$ and $\hat{V}$ are the kinetic and potential energy operators respectively. Considering a one-dimensional system for notational simplicity, the distribution at time u_i can be represented as a set of points distributed on the x-axis according to the initial distribution $\Phi_i(u_i, x_i)$. To carry out the evolution over the time interval ε, we first apply $e^{-\beta\hat{V}/M}$ on $\Phi_i(u_i, x)$ to give $e^{-\beta(V(x)-E_T)/M}$ $\Phi_i(u_i, x)$, where $V(x)$ is measured with respect to some energy E_T. This will imply that in regions of low potential energy, the probability distribution will be enhanced whereas in regions of high potential energy, the distribution will be attenuated (birth/death process). To complete the evolution we must then act using the operator $e^{-\beta\hat{K}/M}$ which results in

$$\sqrt{m/2\pi\varepsilon}\, e^{-m/2\varepsilon (x_{i+1}-x_i)^2}\, e^{-\beta V(x_i)/M}\, \Phi_i(u_i, x_i) . \tag{5}$$

Note that the positions obtained at the end of the time step, x_{i+1}, are Gaussian distributed about the positions x_i at time u_i. This can be interpreted as a diffusion step with diffusion constant $\hbar/2m$. Thus a short-time propagation corresponds to a birth/death step followed by a diffusion step. Repeated application of such short time evolutionary operators will result in convergence to the ground state.

For all but the simplest system, the naive DMC algorithm described above must be made more efficient by introducing importance sampling. Importance sampling biases the random walk towards the most important regions of configuration space by using the information provided by a good approximate wavefunction, usually derived from a VMC calculation. A different formulation of this zero-temperature approach, equivalent to the DMC method, is Green's Function Monte Carlo (GFMC).

Monte Carlo methods require the definition of a probability distribution function that is always positive. In the case of VMC simulations, the modulus squared of the wavefunction provides a positive probability distribution function. In DMC simulations of bosons or distinguishable particles, the nodeless ground state wavefunction can be treated as a probability distribution. In the case of interacting fermions, however, the ground state cannot be assumed to be nodeless. The antisymmetrization requirement for fermions implies that nodes will exist in the wavefunction whenever positions of two fermions with identical spins coincide. Continuity of the wavefunction and its first derivative then implies that the wavefunction must change sign at these nodal planes. Consequently, the interpretation of the ground state wavefunction as a probability distribution is invalid, leading to the well-known 'fermion-sign' problem. Fixed-node methods which are surprisingly accurate though not, in principle, exact, have been developed to circumvent this problem. A very important application of this fixed-node DMC technique has been in deducing the exchange correlation functional for the uniform electron gas, which forms the basis of most density functional and *ab initio* MD calculations[19].

3. Path integral Monte Carlo method

Path integral Monte Carlo (PIMC) techniques allow for simulations of quantum many-body systems in the canonical ensemble (constant number N, volume V and temperature T). The equilibrium properties of a system in the NVT ensemble are determined by the canonical partition function, Q. For a quantum system, Q must be expressed as a trace over the density operator $e^{-\beta\hat{H}}$; evaluation of the trace in the coordinate representation then leads to:

$$Q = \mathrm{Tr}\,\{e^{-\beta\hat{H}}\} = \int d\mathbf{x}\, \langle \mathbf{x} | e^{-\beta\hat{H}} | \mathbf{x} \rangle , \tag{6}$$

where $\mathbf{x}$ is the position vector for the N-particle system. Path integral methods interpret $e^{-\beta\hat{H}}$ as a propagator in imaginary time (note the similarity with DMC) and express the density matrix elements as the functional integral

$$\langle \mathbf{x} | e^{-\beta\hat{H}} | \mathbf{x}' \rangle = \int \mathcal{D}(\mathbf{x}(u)) e^{-S(\mathbf{x}(u))/\hbar} , \tag{7}$$

where the integral represents the sum over all possible paths, $\mathbf{x}(u)$, in imaginary time u which satisfy the condition that $\mathbf{x}(0) = \mathbf{x}$ and $\mathbf{x}(\beta\hbar) = \mathbf{x}$. The weighting of individual paths is given by the exponential of the

action in imaginary time, $S(\mathbf{x}(u))$. Note that only cyclic quantum paths with the same initial and final point can contribute to Q. The classical path is the path of least action[20].

PIMC methods involve finding paths which contribute the most to the partition function. For example, in the discretized path integral approach, any quantum path is represented as a set of configurations, $\{\mathbf{x}_i\}$, at equispaced intervals in imaginary time, $u = 0$, $(\beta\hbar/M)$, $(2\beta\hbar/M)$, ..., $\beta\hbar$. Using this representation, Q for an N-particle system can be written as

$$Q = \frac{1}{N!}\left(\frac{Mm}{2\pi\beta\hbar^2}\right)\int d\mathbf{x}_1\, d\mathbf{x}_2 \ldots d\mathbf{x}_M \times$$

$$\exp\left\{\frac{-Mm}{2\beta\hbar^2}\,(x_{12}^2 + x_{23}^2 + \ldots x_{M1}^2)\right\} \times$$

$$\exp\left\{\frac{-\beta}{M}\,(V(\mathbf{x}_1) + V(\mathbf{x}_2) + \ldots V(\mathbf{x}_M))\right\}, \quad (8)$$

where $\mathbf{x}_{ij} = |\mathbf{x}_i - \mathbf{x}_j|$. The partition function in equation (8) has the same structure as the classical configurational integral with $3NM$ spatial degrees of freedom. The interpretation of the above partition function is, however, somewhat novel. In the classical limit, a particle is characterized by 3 position degrees of freedom. In the discretized path representation, the single quantum particle is replaced by a cyclic polymer of M subunits, with adjacent subunits held by a harmonic interaction; the external potential felt by each subunit is $V(\mathbf{x}_i)/M$. The average extent of the polymer is proportional to the thermal de Broglie wavelength of the particle. Equation (8) can be used directly in conjunction with the Metropolis algorithm to simulate a many-particle quantum system. It is, however, often computationally more efficient to employ alternative representations of the path integral[21]. The common feature of all such PIMC methods is the quantum classical isomorphism – by introducing auxilliary degrees of freedom (such as the $M-1$ additional position degrees of freedom for the polymer subunits), the trace over the density operator is written as a classical configurational integral of much higher dimensionality. The fermion sign problem present in DMC recurs also for the finite temperature formulation and methods analogous to the zero-temperature are currently being devised. An interesting and unsolved problem is whether the imaginary time PIMC formulation can be adapted for real-time problems. While this is one approach towards achieving the tantalizing goal of devising a simulation method for many-body quantum dynamics, so far it has met with little success[21].

PIMC methods have been applied extensively to molecular systems. The best studied system is liquid ^{4}He which shows a Bose–Einstein transition to a superfluid state; simulation results compare very well to the experiment[12]. Good approximation methods for finite temperature fermionic systems have been developed recently and applied to liquid ^{3}He and electronic structure[22,23]. An interesting possibility is combining PIMC methods for nuclei with Car–Parinello techniques for obtaining the electronic structure. While prohibitively expensive at present for bulk systems, it has been applied to CH_5^+. The structure of CH_5^+ has long been controversial with arguments that it is a unique carbonium atom as opposed to the theory that it is the prototype for a nonclassical hyper-coordinate carbocation, with a ground state dominated by 3-centre-2-electron bonding. The combined PIMC and *ab initio* MD calculations indicate that the quantum ground state is dominated by 3*c*-2*e* bonding[24,25].

4. Some applications

Surface adsorption

The importance of surface adsorption, from practical applications in heterogeneous catalysis to theoretical models for phase transitions in two-dimensional systems, does not require emphasis. As a result, classical simulation of surfaces and interfaces is by now a well-developed field[26]. Appreciable quantum effects can, however, be expected for light adsorbates, e.g. H_2, He, Ne, N_2 and CO, specially at low temperatures. One of the first surface adsorption problems to be studied by PIMC was ^{3}He and ^{4}He adsorption on graphite[27]. The quantum simulations corroborated experimental results for the different phase diagrams of the two isotopes and provided interesting insights into the microstructure associated with different phases. In addition, DMC/GFMC calculations have been carried out to explore the zero temperature limit of the He/graphite system[12]. In contrast to atomic substrates, diatomic molecules can exhibit a range of orientational transitions. For example, N_2/graphite shows a herringbone transition; PIMC simulations have quantified that the lowering of the transition temperatures due to quantum effects is 10% (30 K) (ref. 28). The CO/graphite system is analogous to the N_2 adsorption problem except for a heat capacity anomaly at approximately 5 K. Recent PIMC simulations have shown that this must correspond to the head-to-tail ordering transition for the two-dimensional CO system[29]. To my knowledge, there have been no zero-temperature studies of molecular adsorption, largely because interest in this area centres on finite temperature phase transitions.

Solvated electrons

The solvated electron, a 'free' electron trapped in a cavity formed by solvent molecules, plays an important role in a variety of chemical phenomena. The hydrated

electron has been shown to be a transient species of crucial importance in solution photochemistry since its identification more than 30 years ago[30,31]. The solvated electron is central to the metal–insulator transitions observed in alkali metal–ammonia solutions and related systems. The localized versus extended states responsible for the metal–insulator transition are also connected to electron mobilities in fluids and other disordered media; therefore the general problem of excess electron mobilities in a variety of solvents has attracted much theoretical and experimental attention[32–34]. The structure of a solvated electron in a fluid will be determined by the competition between two factors: a tendency to delocalize and occupy as large a volume as possible in order to minimize the kinetic energy and a tendency to minimize potential energy by optimizing electron–solvent interactions. In the case of the dominant contribution to the electron–solvent interaction being an excluded volume or repulsion interaction, the electron will tend to localize in regions of low fluid density. If the attractive interactions can be enhanced in these low density traps (for example, by the presence of oriented solvent dipoles) then the size of the cavity can be substantially reduced. The fact that the characteristics of solvated electron systems will depend on this type of complex interplay between a variety of factors, makes simulations a virtual necessity. Different simulation techniques can then be used to provide complementary information on these systems.

Among the best-studied solvated electron systems, both from an experimental and simulation perspective, are the alkali metal–ammonia solutions which have a long experimental history[35]. Alkali metals dissolve in liquid ammonia and, at very low concentrations, form a light blue solution. Spectroscopic and other evidences indicate that, as in the case of F-centres in alkali halides, the blue colour is due to the optical spectrum of an isolated solvated electron. As the concentration of metal is increased, the magnetic susceptibility falls, indicating that some type of spin pairing process is in operation. However, as the metal concentration increases, a metal insulator transition takes place and a bronze-coloured liquid metal is formed. At still higher concentrations, metallic solid compounds are formed. The dilute limit is ideally treated by PIMC methods[36]. The results show the trapping or localization of single electrons in solvent cavities with an effective size of about 4 Å. In fact, a transition from a delocalized to a localized, trapped state is seen as solvent concentration is increased. The results of the simulation agree well with experiment as well as with predictions of the RISM-polaron theory[37]. The metallic limit with high electron concentration can be treated by Car–Parrinello methods[38–40]. The intermediate regime, especially where spin-pairing occurs, can be treated by both approaches. In the spin-pairing regime, the simulations show that electron-pairs form singlet states which occupy a peanut-shaped cavity with the two peaks in the electron density separated by 7 Å. The triplet state is unstable with respect to the singlet state by approximately 0.6 eV. Thus, this series of simulations on the alkali metal–ammonia solutions has provided considerable insight into the microstructure and dynamics associated with the metal–insulator transition.

Quantum clusters

Clusters have attracted much attention by virtue of being small systems which bridge the transition from molecular to bulk properties[41–44]. While clusters can show properties similar to those of bulk matter, e.g. collective behaviour analogous to a phase transition, they are sufficiently small to be studied at the same level of microscopic detail as molecular systems. In this section, some of the applications of QMC methods to quantum clusters are summarized. Quantum clusters denote small, finite atomic or molecular systems (about 10–1000 atoms) where the nuclei have appreciable quantum character. Recent experiments on rare-gas–SF_6 clusters have added to the interest in quantum clusters[45]. Electronic structure aspects, of special relevance to metallic and semiconductor clusters, are not considered here. It should be pointed out that cluster simulations have played an important role in the development of QMC methods; for example, one of the first applications of VMC and GFMC methods was to helium clusters to test the reliability of liquid drop models for clusters[45].

Atomic clusters, such as those of He, Ne, H_2 and D_2 have been very useful in understanding quantum effects on phase transitions[46–54]. For example, ^4He_n with $n > 60$ shows clear remnants of the bulk superfluid transition and QMC simulations can provide a corresponding microscopic model[53]. Bulk melting has its cluster analogue and has been studied in clusters with a view to understanding the role played by quantum fluctuations in modifying phase transition characteristics. For example, Figure 1 shows the lowering of the position and height of the specific heat curve for a Ne_{13} cluster due to quantum effects[48]. Increasing quantum delocalization can be shown to result in a cluster solid–liquid transition analogous to the thermal melting transition[55]. The effects of such delocalization can be seen in Figure 2, where the angular distributions for the Ne_{13}, $(para\text{-}H_2)_{13}$ and $(ortho\text{-}D_2)_{13}$ are compared with those of a classical thirteen atom Lennard–Jones cluster[49]. A purely quantum analogue of the classical binary phase separation can be shown to occur in isotopically mixed clusters using PIMC methods[56]. Figure 3 shows the density profiles for the two isotopic species in a mixed *para*-H_2/*ortho*-D_2 cluster; the heavier isotope can be seen to be preferentially located in the cluster interior.

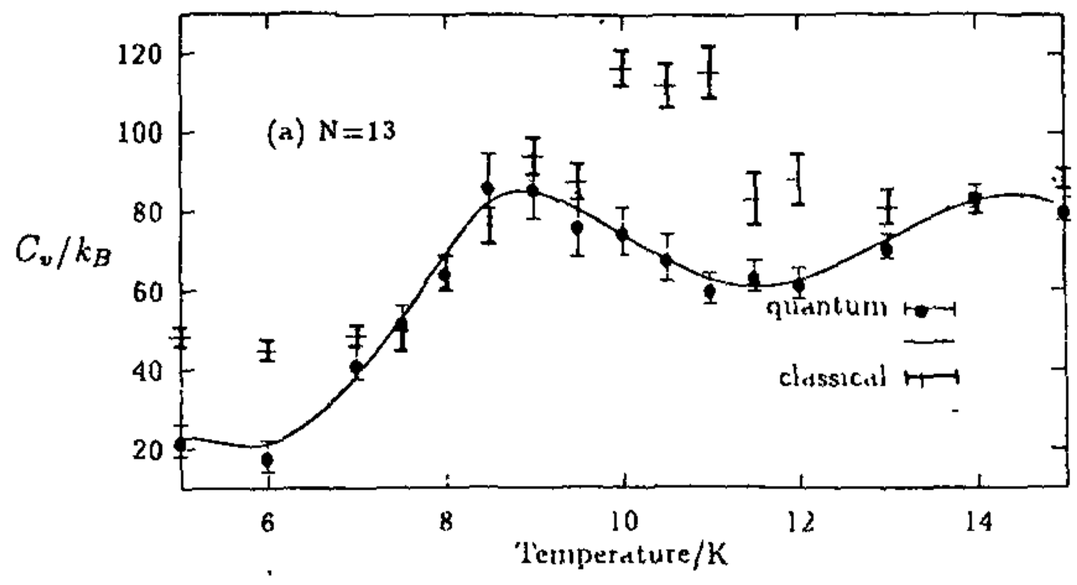

Figure 1. The specific heat, C_v/k_B, as a function of temperature for a Ne_{13} cluster. Results from path integral quantum Monte Carlo and classical simulations are compared.

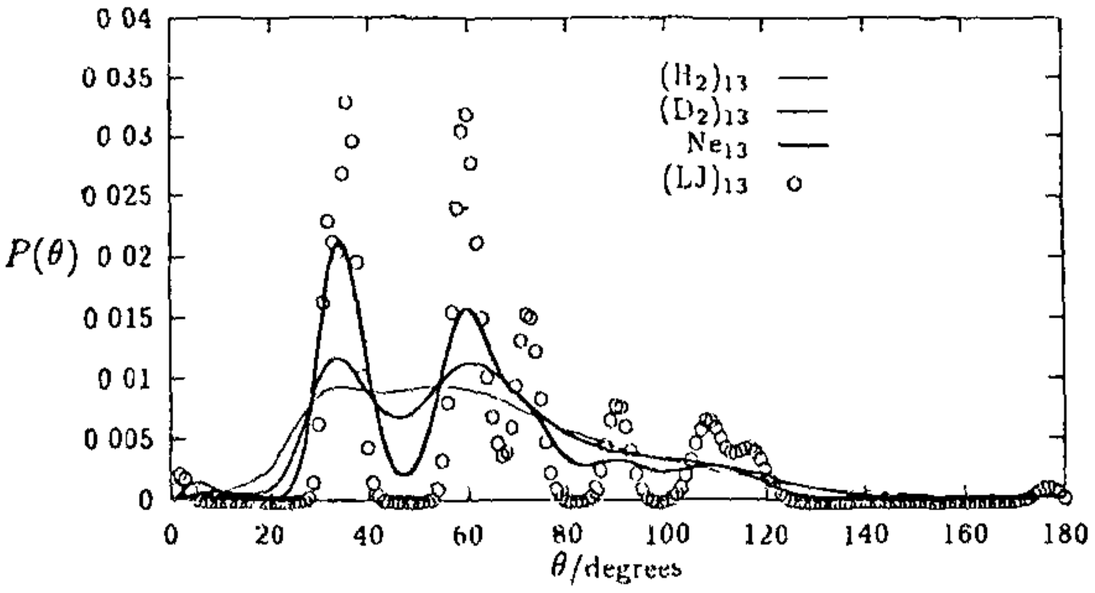

Figure 2. Angular distributions, $P(\theta)$, for thirteen atom clusters at 5 K. The distribution for the classical Lennard–Jones cluster, $(LJ)_{13}$, is compared with that for quantum clusters of Neon, *para*-H_2 and *ortho*-D_2. The latter two species can be treated as pseudo-atomic systems interacting via a spherically symmetric pair potential at low temperatures. The peak at 60° is characteristic of the icosahedral symmetry of small Lennard–Jones clusters.

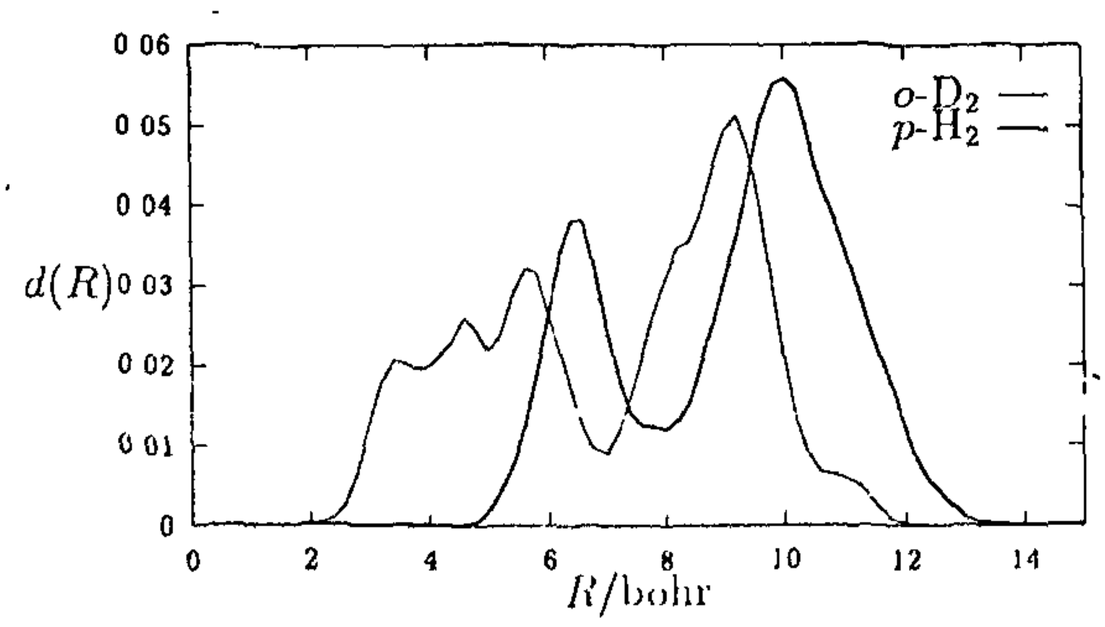

Figure 3. Radial density profiles, $d(R)$ for the two isotopic species in the $(P\text{-}H_2)_9(O\ D_2)_9$ cluster at 2.5 K. The radial density profile is a measure of the probability of finding a particle of a particular species at a distance R from the centre of mass of the cluster

A second category of clusters with large quantum effects are the so-called solvent clusters such as $(H_2O)_n$, $(NH_3)_n$ and $(HF)_n$. Understanding the structure and dynamics of such systems is of particular importance from the point of view of solvation, liquid structure and hydrogen bonding. Small aggregates of two, three or four monomers have been intensively studied by QMC methods (mostly DMC). Such studies are very valuable from the point of view of deriving accurate intermolecular potentials by comparison and fitting to spectroscopic data.

Electron transfer

Electron transfer is fundamental to a variety of chemical and biochemical processes. An electron transfer process may be represented as:

$$\text{Acceptor(A)} + \text{Donor}(D^-) \rightarrow A^- + D, \qquad (9)$$

where A and D may be ions or molecules and the reaction takes place in a dielectric solvent. A simple model for electron transfer envisages the electron as being trapped on one of two wells, localized on either A or D, with shapes and relative energies of the two wells determined by the classical degrees of freedom of the nuclei composing A, D and solvent. The electron transfer process between the two wells corresponds to a tunnelling transition. In the limit that the coupling of the electronic (quantum) and classical degrees of freedom is weak, the rate constant for electron transfer can be related to the tunnelling splitting and a Franck–Condon factor. PIMC calculations can be used to calculate the magnitude of the tunnelling splitting[57]. The computation of the tunnelling splitting assumes a large scale separation between the frequency of tunnelling (or inter-well) and intra-well motions. Tunnelling paths correspond to quantum paths which connect the two wells. The fraction of imaginary time spent in the barrier region along such a path will be small because the potential energy in the barrier region is high. This type of rapid process or instanton is then said to correspond to a kink in the quantum path and the tunnelling constant can be related to the free energy required to create a kink in the quantum path. Estimation of this free energy can be accomplished in MC simulations by standard thermodynamic integration methods. The Franck–Condon factor can be related to fluctuations in the relative energy of the two potential wells and estimated from classical MC or MD simulations. An ambitious application of this approach has been in explaining some of the unusual features of the primary electron transfer step in bacterial photosynthesis[58,59]. It should be noted that the above approach estimates a dynamical quantity, the rate constant, in terms of equilibrium thermodynamic averages[60].

This can be shown to be a plausible approximation for many systems and has been applied to calculate rates for quantum processes such as proton transfer and hydrogen chemisorption[61,62].

1. Dirac, P. A. M., *Proc. R Soc.*, 1929, **123**, 714–735.
2. Franks, F., *Water, A Comprehensive Treatise*, Plenum Press, New York, 1975.
3. Farantos, S. C., Kapetanakis, S. and Vegiri, A., *J. Phys. Chem.*, 1993, **97**, 12158–12166
4. Parsonage, N. G. and Stavely, L. A. K., *Disorder in Crystals*, Clarendon Press, Oxford, 1978.
5. Allen, M P. and Tildesley, D. J., *Computer Simulation of Liquids*, Clarendon Press, Oxford, 1987.
6. Putnis, A., *Introduction to Mineral Sciences*, Cambridge University Press, 1992.
7. McCammon, J. A. and Harvey, S C., *Dynamics of Proteins and Nucleic Acids*, Cambridge University Press, London, 1987.
8. Maitland, G. C., Rigby, M., Smith, E. B. and Wakeham, W. A., *Intermolecular Forces: Their Origin and Determination*, Clarendon Press, Oxford, 1991.
9. Kranenodonk, W. G. T. and Frenkel, D., *Mol. Phys.*, 1991, **72**, 679–713
10. Payne, M. C., Teter, M. P., Allan, D. C., Arias, T. A. and Joannopoulos, J. D., *Rev Mod Phys.*, 1992, **64**, 1045–1097.
11. Ceperley, D. and Alder, B., *Science*, 1986, **231**, 555–560.
12. Schmidt, K. E. and Ceperley, D. M., in *The Monte Carlo Method in Condensed Matter Physics* (ed. Binder, K.), Springer, Berlin, 1992.
13. Hammond, B. L., Lester, W. A. and Reynolds, P. J., *Quantum Monte Carlo Methods in Ab Initio Quantum Chemistry*, World Scientific, Singapore, 1994.
14. Suhm, M A. and Watts, R. O., *Phys. Rep.*, 1991, **204**, 293–329
15. Metropolis, N. and Ulam, S., *J. Am. Stat. Assoc.*, 1949, **44**, 335–354.
16. Anderson, J. B., *J. Chem. Phys.*, 1975, **63**, 1499–1053; *J. Chem. Phys.*, 1980, **73**, 3897–4001.
17. Fahy, S., Wang, X. W. and Louie, S. G., *Phys. Rev.*, 1990, **B42**, 3503–3522.
18. Whaley, K. B., *Int. Rev. Phys. Chem.*, 1994, **13**, 41–84.
19. Ceperley, D. M. and Alder, B. J., *Phys. Rev. Lett*, 1980, **45**, 566–569; Ceperley, D. M., *Phys. Rev.*, 1978, **B18**, 3126–3155.
20. Feynman, R. P., *Statistical Mechanics*, Addison-Wesley, 1972.
21. Doll, J. D., Freeman, D. L. and Beck, T. L., *Adv. Chem. Phys.*, 1990, **78**, 61–127.
22. Ceperley, D. M, *J. Stat. Phys*, 1991, **63**, 1237–1267.
23. Ceperley, D. M., *Phys. Rev Lett.*, 1992, **69**, 331–334.
24. Scuseria, G. A., *Nature*, 1993, **366**, 512–514.
25 Marx, D. and Parrinello, M, *Nature*, 1995, **375**, 216–218.
26. Nicholson, D. and Parsonage, N., *Computer Simulation and the Statistical Mechanics of Adsorption*, Academic Press, New York, 1982.
27. Abraham, F. F. and Broughton, J. Q., *Phys. Rev. Lett.*, 1987, **59**, 64–67.
28. Marx, D., Opitz, O., Nielaba, P. and Binder, K., *Phys. Rev. Lett.*, 1993, **70**, 2908–2911.
29. Marx, D, Sengupta, S., Nielaba, P. and Binder, K, *Phys. Rev. Lett.*, 1994, **72**, 262–265.
30. Rossky, P. J and Schnittker, J, *J. Phys. Chem.*, 1988, **92**, 4277–4285
31. Hart, E. J. and Boag, J. W., *J. Am. Chem. Soc.*, 1962, **84**, 4090–4095.
32. Chandler, D. and Leung, K, *Annu. Rev. Phys. Chem*, 1994, **45**, 557–592.
33. Liu, Z and Berne, B. J., *J. Chem. Phys*, 1993, **99**, 9054–9064.
34. Fois, E. S, Selloni, A., Parrinello, M. and Car, R., *J. Phys Chem.*, 1988, **92**, 3268–3273.
35. Thompson, J. C., in *Metal–Non Metal Transitions* (eds Edwards, P. P. and Rao, C. N. R), Taylor and Francis, London, 1985.
36. Sprik, M, Impey, R. and Klein, M. L., *Phys. Rev Lett.*, 1986, **56**, 2326–2329.
37. Chandler, D., in *Liquids, Freezing and the Glass Transition* (eds Hansen, J. P., Levesque, D. and Zinn-Justin, J.), Elsevier, Amsterdam, 1991.
38 Deng, Z., Martyna, G. J. and Klein, M L., *Phys. Rev. Lett.*, 1992, **68**, 2496–2499.
39. Martyna, G. J, Deng, Z. and Klein, M. L., *Chem. Phys.*, 1993, **98**, 555–563.
40. Deng, Z., Martyna, G. J. and Klein, M. L., *J. Chem. Phys*, 1994, **100**, 7590–7599.
41. Berry, R. S., *J. Phys. Chem.*, 1994, **98**, 6910–6918.
42. Sugano, S, *Microcluster Physics*, Springer, Berlin, 1991.
43. Nayak, S. K., Ramaswamy, R. and Chakravarty, C., *Phys. Rev.*, 1995, **E51**, 3376–3380.
44. Nayak, S. K., Ramaswamy, R. and Chakravarty, C., *Phys. Rev. Lett*, 1995, **74**, 4181–4184.
45. Goyal, S., Schutt, D L. and Giacinto Scoles, *J. Chem. Phys.*, 1995, **102**, 2302–2324.
46. Pandharipande, V. R., Zabolitsky, J. G., Piper, S. C., Wiringa, R. B. and Helmbrecht, U., *Phys. Rev. Lett.*, 1983, **50**, 1676–1679.
47. Chakravarty, C., *J. Chem. Phys.*, 1993, **99**, 8038–8043.
48. Chakravarty, C., *J. Chem. Phys.*, 1995, **102**, 956–962.
49. Chakravarty, C., *Mol. Phys.*, 1995, **84**, 845–852.
50. McMahon, M. A, Barnett, R. N. and Whaley, K. B., *J. Chem. Phys.*, 1993, **99**, 8816–8829.
51. Scharf, D., Martyna, G. J. and Klein, M. L., *J. Chem Phys.*, 1993, **99**, 8997–9012.
52. Scharf, D., Klein, M. L. and Martyna, G. J., *J. Chem. Phys.*, 1992, **97**, 3590–3599.
53. Sindzingre, P., Ceperley, D. M. and Klein, M. L., *Phys Rev. Lett.*, 1991, **67**, 1871–1874.
54. Scharf, D., Martyna, G. J. and Klein, M. L., *Chem. Phys. Lett.*, 1992, **197**, 231–235.
55. Chakravarty, C., *J. Chem. Phys.*, in press.
56. Chakravarty, C., *Phys. Rev. Lett*, 1995, **75**, 1727–1730.
57. Marchi, M and Chandler, D., *J. Chem. Phys*, 1991, **95**, 889–894.
58. Marchi, M., Gehlen, J. N., Chandler, D. and Newton, M, *J. Am. Chem. Soc.*, 1993, **115**, 4178–4190.
59. Mak, C. H. and Egger, R., *Phys. Rev.*, 1994, **E49**, 1997–2008.
60. Wang, J. and Wolynes, P., *Chem. Phys Lett*, 1993, **212**, 427–432.
61. Voth, G. A., Chandler, D. and Miller, W. H., *J. Chem. Phys.*, 1989, **91**, 7749–7760.
62. Mills, G. and Jonsson, H, *Phys. Rev. Lett.*, 1994, **72**, 1124–1127.

Received 18 May 1995; revised accepted 19 November 1995